Available online at www.sciencedirect.com
SCIENCE DIRECT®
Journal of Organometallic Chemistry 669 (2003) 154–163
Journal of Organometallic Chemistry
www.elsevier.com/locate/jorganchem

Modelling nucleophilic substitution at silicon using solution ^{19}F-NMR chemical shift, $^{1}J_{Si-F}$ and $^{2}J_{C-F}$ coupling constant data of pentacoordinate silicon compounds. Correlation with other magnetic nuclei and X-ray structures

Alan R. Bassindale [a,*], Yuri I. Baukov [b], Moheswar Borbaruah [a], Simon J. Glynn [a], Vadim V. Negrebetsky [b], David J. Parker [a], Peter G. Taylor [a,*], Robert Turtle [a]

[a] Department of Chemistry, Open University, Walton Hall, Milton Keynes MK7 6AA, UK
[b] Department of General and Bioorganic Chemistry, Ostrovityanov St. 1, Moscow 117997, Russia

Abstract

Solution $^{1}J_{Si-F}$ and $^{2}J_{C-F}$ NMR coupling constant and ^{19}F-NMR chemical shift data have been analysed in a series of pentacoordinate silyl monofluoride complexes used to model nucleophilic substitution at silicon. Patterns in the data reveal strong correlations between both coupling constants and ^{19}F-NMR chemical shifts and the degree of substitution displayed by each. Excellent correlation is obtained between the new data and our previous ^{13}C- and ^{29}Si-NMR studies to further confirm the validity of the NMR technique for structural correlation in solution. By pooling the X-ray crystal structures of a large number of compounds of this class from both our own results and the literature we are able to provide a possible explanation for some of the trends in the NMR data we observe in solution.

Keywords: Silicon; Pentacoordinate; Fluorine NMR; Coupling constant; X-ray study; Nucleophilic substitution; Structural correlation

1. Introduction

The technique of mapping the trajectory of nucleophilic substitution by analysing and sequencing compound structures has long been established. Each structure is treated as though it represents a model of the substitution process frozen at a particular point on the reaction coordinate. Thus a series of suitably-sequenced structures reveals the reaction profile as a series of 'snapshots'. Dunitz et al. [1] first developed the technique of *structural correlation* whereby a series of suitable X-ray crystal structures could be analysed by monitoring changes to key geometric data, usually inter-atom distances, to allow the gradual deformation about the modelled reaction centre to be observed. Our early studies [2] and those of Pestunovich [3] in examining the crystal structures of related *N*-(amidomethyl)-halosilanes (**1**) (Scheme 1) first revealed that the nucleophile–silicon (Nu–Si) and silicon-leaving group (Si–X) bond lengths are related by a hyperbolic function with a regular change in the position of the silicon atom in respect to the plane of the three equatorial carbon atoms. While this technique proved powerful in the solid state, its wider application was limited by the need for crystalline samples suitable for X-ray crystal structure analysis.

We have subsequently developed the technique of *solution phase mapping* for the structural correlation of silicon in solution by analysing the ^{13}C- and ^{29}Si-NMR chemical shifts of a variety of 1-dimethylsilyl-2-pyridone complexes (**2**) [4]. Each intramolecular pentacoordinate species represents a particular point on the reaction pathway with the hyper-coordinating group as the nucleophile. The different stable hyper-coordinate structures are obtained by varying the nucleophilic properties of the pyridone ligand (i.e. **2.1**–**2.6**) and changing the leaving group substituent on the silicon (i.e. **a**–**d**).

* Corresponding authors. Fax: +44-1908-85-8327.
E-mail address: p.g.taylor@open.ac.uk (P.G. Taylor).

0022-328X/03/$ - see front matter © 2003 Elsevier Science B.V. All rights reserved.
doi:10.1016/S0022-328X(03)00009-3

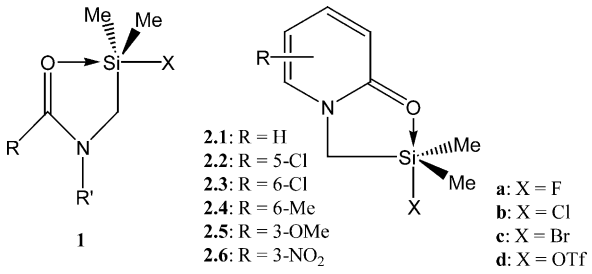

Scheme 1.

Since the ^{13}C-NMR chemical shifts of the pyridone ring carbons are found to change in a linear and concerted fashion [5] as the extent of Nu–Si bond formation increases, we can use these chemical shift changes to determine the extent of substitution displayed by reference to 'model' compounds representing 0 and 100% substitution. The ^{29}Si-NMR chemical shift is especially susceptible to changes in the coordination state at silicon and this allows the degree of pentacoordination to be calculated, again with reference to model compounds.

The technique is versatile and further investigations using 2-thiopyridone (**3.1**–**3.3**) [6], 2-quinolinone (**4**) [4] and urea (**5**) [7] complexes (Scheme 2) have allowed around 40 points across the entire reaction coordinate to be modelled. This has allowed the pathway from tetracoordinate (unsubstituted) to tetracoordinate (fully substituted) silicon to be revealed as proceeding via a fully pentacoordinate, trigonal-bipyramidal intermediate involving 50% silicon–nucleophile (Si–Nu) formation (Fig. 1).

We have also applied the solid state correlation approach to complexes **4a**–**d** [8]. Analysis of their X-ray crystal structures reveals a similar pattern to that observed for complexes **1** with a direct correlation between parameters in the solid and solution phases.

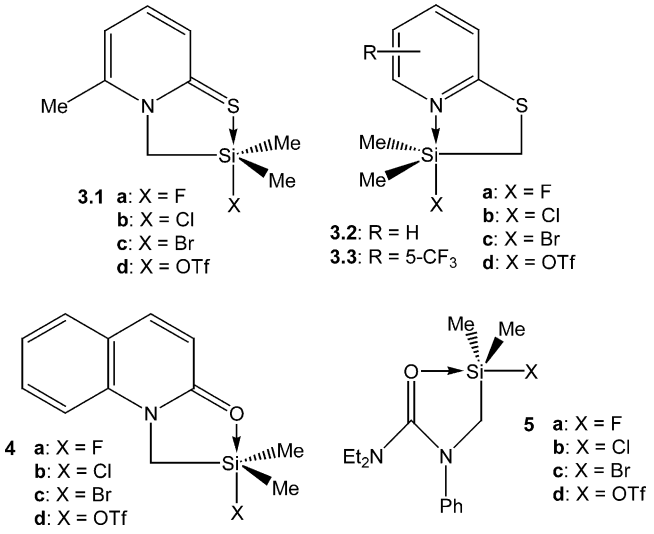

Scheme 2.

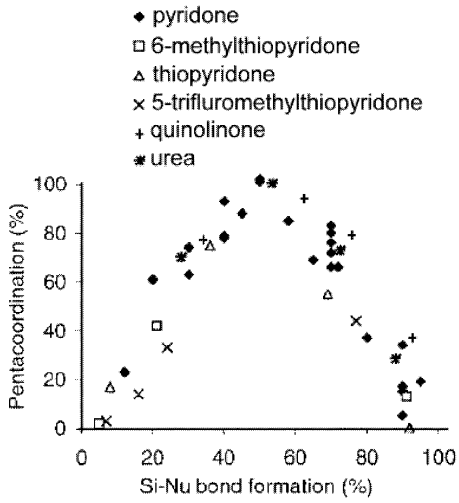

Fig. 1. The plot of percentage of pentacoordination against percentage of Nu–Si bond formation as determined by NMR in solution for pentacoordinate silicon complexes types **2**–**5**.

In this paper we will focus on many of the pentacoordinate silyl fluorides used in previous studies and present new ^{19}F-NMR solution phase NMR chemical shift data. In addition we shall refer to suitable examples in the literature which confirm how changes in the ^{19}F-NMR chemical shift, the $^{1}J_{Si-F}$ and various $^{2}J_{C-F}$ coupling constants are closely related to the extent of substitution in such complexes and can therefore be used alongside ^{13}C- and ^{29}Si-NMR data as indicators of their coordination state and degree of substitution at silicon.

2. Results and discussion

Table 1 shows selected NMR chemical shift and coupling constant data for our previously reported silyl fluoride complexes **2.1a**–**2.6a**, **3.1a**–**3.3a**, **4a** and **5a**. The figure *percentage of Nu–Si bond formation* previously calculated from the ^{13}C-NMR chemical shift data for each complex is a convenient and tested measure of the extent of substitution and so is a suitable parameter against which to test our coupling constant and ^{19}F-NMR chemical shift data.

In these examples the most electronegative groups, the nucleophile (N, O or S) and leaving group (F, Cl, Br or OTf), tend to occupy the apical positions. The remaining methyl and methylene groups occupy equatorial positions around the silicon. It is well known that the apical groups tend to have longer bond lengths to the silicon than if they were in an equatorial position or the silicon were tetracoordinate [9].

Fig. 2 shows a good linear correlation ($R = 0.92$) between the ^{19}F-NMR chemical shift and percentage of Nu–Si bond formation considering the range of compounds used. The trend of the ^{19}F-NMR chemical shift to move to lower field with increased substitution is

Table 1
Percentage of Si–O bond formation, ^{19}F-NMR chemical shift (ppm) plus $^{1}J_{Si-F}$ and $^{2}J_{C-F}$ NMR coupling constant data (Hz) for silyl fluoride complexes **2**–**5**

Compound	Percentage of Nu–Si bond formation	δ ^{19}F (ppm)	$^{1}J_{Si-F}$ (Hz)	$^{2}J_{C-F}$ (Si–CH_2) (Hz)	$^{2}J_{C-F}$ (Si–CH_3) (Hz)	Reference
2.1a	30	−116.7	256.8	44.0	25.0	[4]
2.2a	30	−123.0	259.8	41.4	19.4	[4]
2.3a	40	n/m	257.8	46.6	19.4	[4]
2.4a	40	−105.7	252.9	50.5	27.2	[4]
2.5a	20	−122.5	258.8	40.2	23.3	[4]
2.6a	12	n/m	272.5	29.8	18.1	[4]
3.1a	5	−150.2	281.3	23.7	14.6	[6]
3.2a	8	−142.5	275.8	22.0	16.5	[6]
3.3a	7	−155.5	280.3	18.4	14.7	[6]
4a	35	−114.2	254.3	47.5	23.8	[4]
5a	29	−120.5	258.8	44.3	24.8	[7]

n/m, Not measured.

indicative of the apical fluorine's increasing ionic character as its bond to silicon weakens and lengthens under the influence of the approaching nucleophile. For example, complex **6** shows a single ^{19}F-NMR chemical shift at −137.7 ppm for the fluorines attached to the tetracoordinate silicon [10] while in the pentacoordinate complex **7** at −80 °C, the equatorial fluorines appear at −142.2 ppm largely similar to **6**. However, the non-bridged apical fluorines are slightly de-shielded at −115.7 ppm and the fluoride ion bridging the two silicons appears at −70.11 ppm. The crystal structure of **7** shows that the Si–F bridging bonds are 0.3–0.4 Å longer and therefore weaker and more ionic than the non-bridging Si–F bonds.

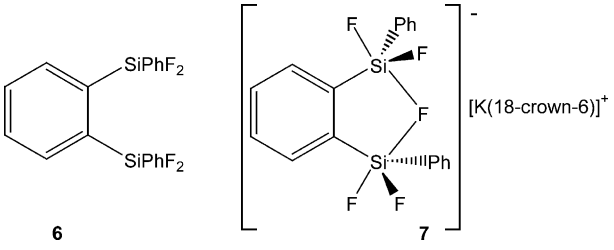

Scheme 3.

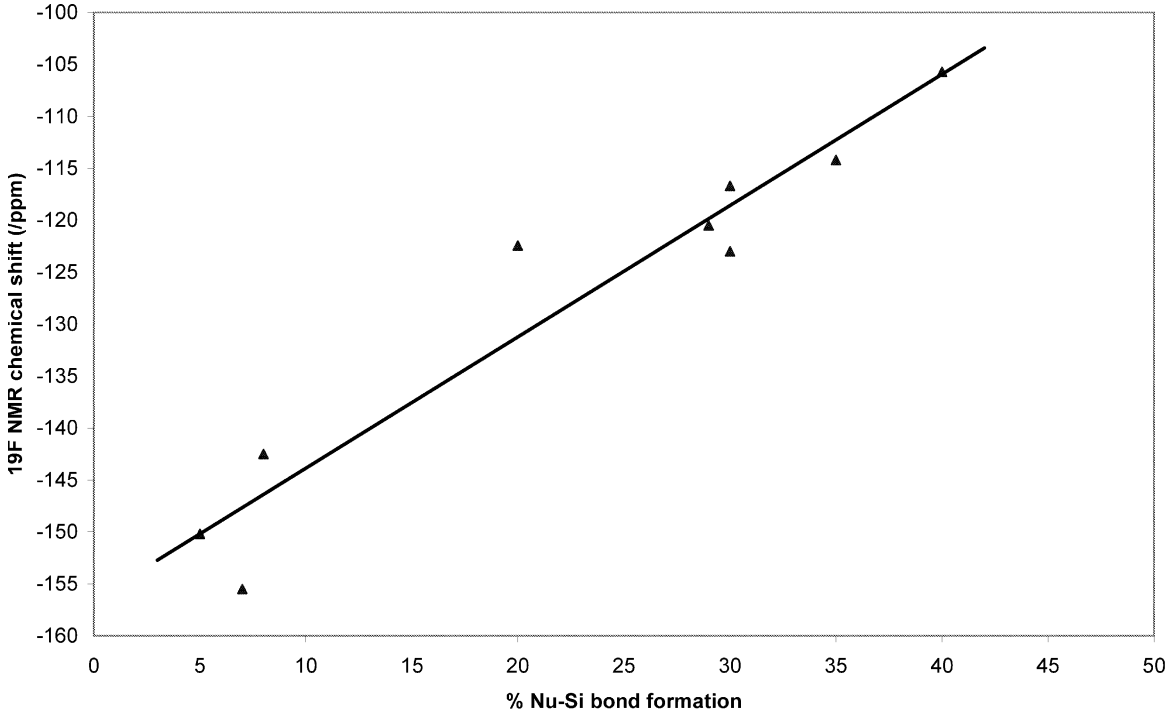

Fig. 2. The plot of ^{19}F-NMR chemical shift (ppm) against percentage of Nu–Si bond formation determined by NMR in solution for silyl fluoride complexes types **2**–**5**.

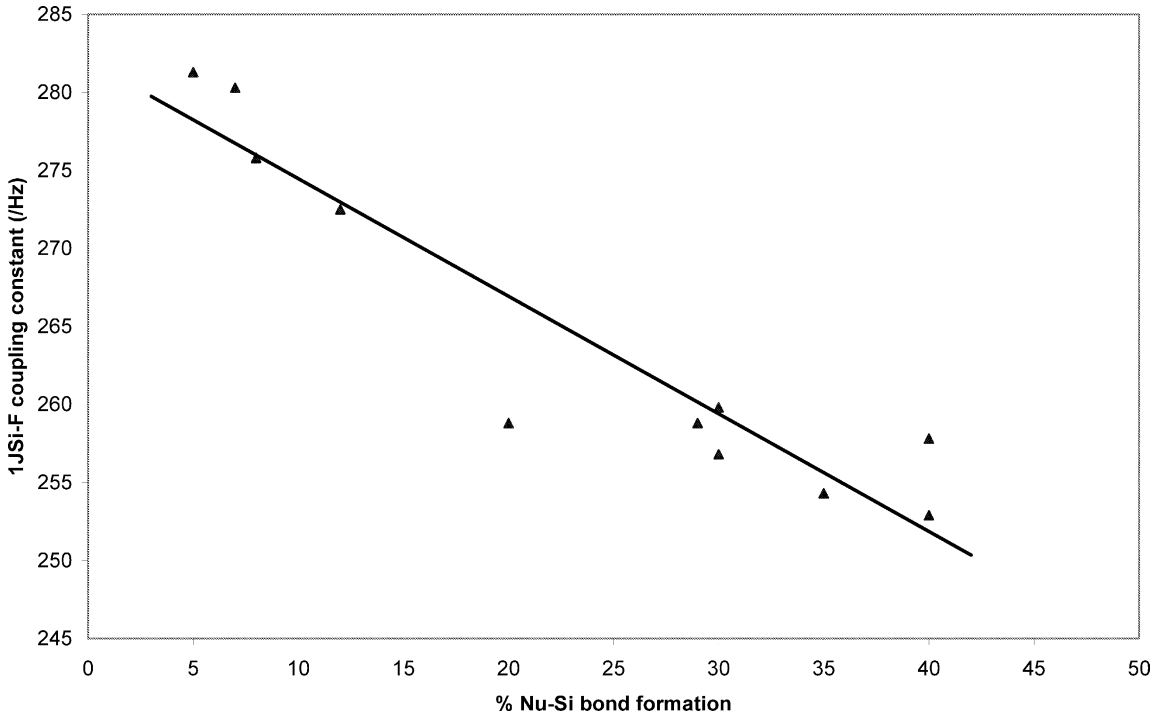

Fig. 3. The plot of $^{1}J_{Si-F}$ NMR coupling constant (Hz) against percentage of Nu–Si bond formation determined by NMR in solution for silyl fluoride complexes types **2**–**5**.

Fig. 3 shows a similar linear relationship between the $^{1}J_{Si-F}$ coupling constant and percentage of Nu–Si bond formation. While the hybridisation state of a pentacoordinated silicon remains a source of debate due to the unclarified role of its d orbitals in hyper-coordinate bonding, it is reasonable to assume that the proportion of s-character is less in the axial bonds of a pentacoordinate silicon than in a tetracoordinate sp^3 silicon and presumably the extent of s-character in such bonds decreases the greater the degree of pentacoordination.

A decrease in the s-character of the Si–F bonding orbital as it becomes axial during substitution would therefore hinder the major Fermi contact through-bond mechanism of coupling and so lead to a lower coupling constant.

Holmes' crystal structure and $^{1}J_{Si-F}$ coupling constant studies of anionic, pentacoordinate diorganotrifluorosilicates [11], such as **8**, showed that although the axial Si–F bond lengths in the solid state were longer than the equatorial ones they gave the larger $^{1}J_{Si-F}$ NMR coupling constants. Nevertheless both coupling constants are presumably smaller than those in tetracoordinate Si–F bonds. Clearly the magnitude of the Fermi mechanism for Si–F coupling is different for axial and equatorial fluorines such that the magnitude of the coupling constant is not solely controlled by the Si–F bond length or percentage of s-character. Therefore, correlating $^{1}J_{Si-F}$ coupling constants to the degree of substitution can only be performed using like-for-like axial, trigonal-bipyramidal Si–F groups.

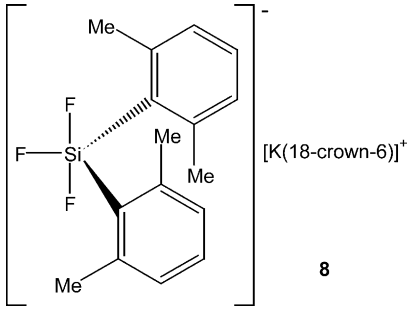

8

Scheme 4.

While there may be a number of possible mechanisms to explain our result, and some interdependence or combination of them cannot be ruled out, the key observation we have made is that there is a linear relationship between percentage of Nu–Si bond formation and $^{1}J_{Si-F}$ NMR coupling constant in our series of compounds.

Fig. 4 shows the relationship between the percentage of Nu–Si bond formation and the two-bond $^{13}C-^{19}F$ coupling constants for the equatorial CH_2 and CH_3 groups attached to the silicon. The magnitude of the coupling constant of the $Si-CH_2$ group increases more quickly with percentage of Nu–Si bond formation than for the $Si-CH_3$ groups. Both plots are curves and if extrapolated appear to reach coupling constant maxima close to 50% reaction.

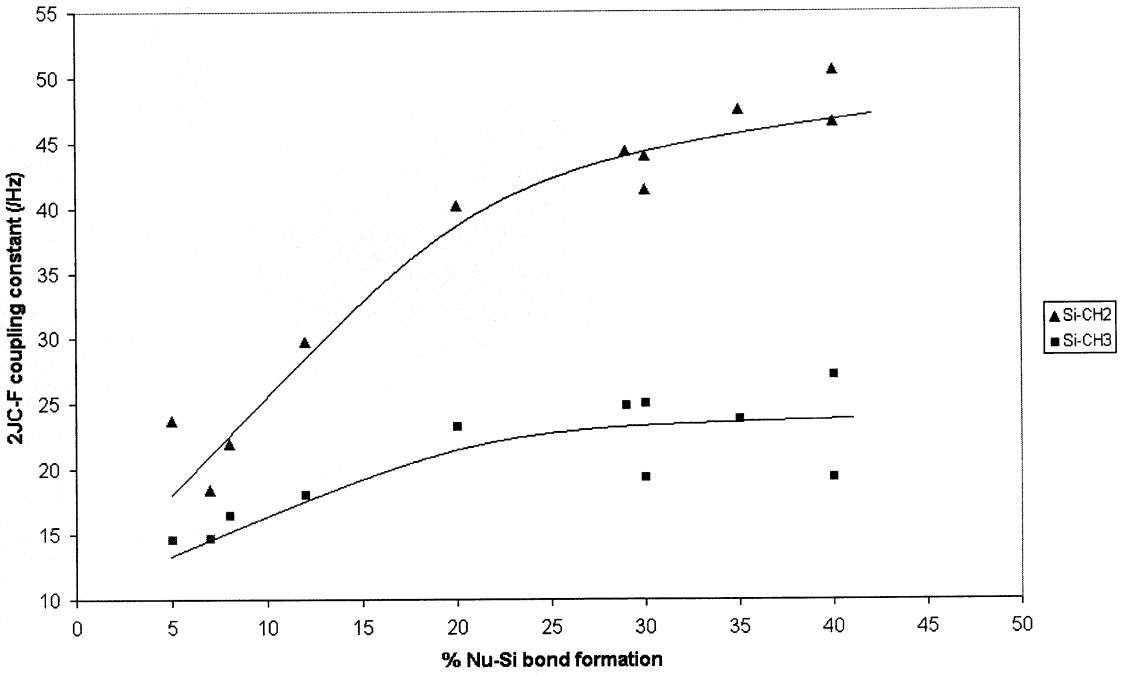

Fig. 4. The plot of $^{2}J_{C-F}$ NMR coupling constant (Hz) against percentage of Nu–Si bond formation determined by NMR in solution for silyl fluoride complexes types **2**–**5**.

As all the silyl–fluoride complexes prepared have a percentage of Nu–Si bond formation less than 50%, we are unable to examine how the $^{2}J_{C-F}$ coupling constants change at greater extents of reaction than this. However, at extents of reaction greater than 50% we would expect the $^{2}J_{C-F}$ coupling constants to decrease with Nu–Si bond formation. This is consistent with formation of a fluoride ion as it leaves the bonding sphere, with the value tending ultimately to zero as it moves out of measurable coupling range. Fig. 3 also shows that at 0% reaction, the fluorine has a similar $^{1}J_{Si-F}$ coupling constant to that expected for the tetrahedral sp^3 hybridised silicon.

The mechanism of spin–spin coupling is more complex for two bond couplings than for one-bond couplings as there are more variables and more than one dominant coupling component. The increase in the $^{2}J_{C-F}$ coupling constant we observe for Si–CH_2 and, to a lesser extent, Si–CH_3 carbons can most probably be attributed to the changing through-space coupling component. This is because we might expect the other major through-bond Fermi coupling component to be increasingly hindered by the reduced s-character of the axial bonding orbitals and the decreasing C–Si–F bond angles as the modelled substitution takes place.

The crystal structures of complexes **4a**–**d** [8] each show a trigonal-bipyramidal geometry at the silicon with different degrees of distortion (i.e. $\theta_{O-Si-X} < 180^{\circ}$, $\Sigma\,\theta_{C-Si-C} < 360^{\circ}$ and $\theta_{X-Si-C} \neq 90^{\circ}$). In particular, the X–Si–CH_2 bond angle decreases in sequential order from **4a** to **4d** more than the mean of the two X–Si–CH_3 bond angle resulting in a net deformation of the Si–X axis towards the Si–CH_2 group and away from the Si–CH_3 groups during the 'substitution'. This phenomenon may help explain why the $^{2}J_{C-F}$ coupling constant increases more rapidly during the first half of the 'reaction' for the Si–CH_2 carbon than for the Si–CH_3 carbons of our fluorosilane complexes.

To demonstrate that the patterns we have observed are quite widespread we have examined the NMR data of four analogous silyl fluoride complexes (**9**–**12**) previously reported by ourselves but not studied by solution phase mapping. Additional NMR data from that already published has been obtained to allow this comparison to be undertaken. Table 2 summarises the key chemical shift and coupling constant data for compounds **9**–**12**. Compound **11** contains two silicon centres and data for both are presented here.

Table 2
^{19}F-NMR chemical shift (ppm) and $^{1}J_{Si-F}$ coupling constant (Hz) data for silyl fluoride complexes **9**–**12**

Compound	Reference	δ ^{19}F (ppm)	$^{1}J_{Si-F}$ (Hz)
9	[4]	−128.7	260.3
10	[4]	−141.6	269.0
11 (tetra.)	[12]	−159.8 [a]	287.0
11 (penta.)	[12]	−116.7 [a]	257.0
12	[13]	−139.0 [a]	266.8

[a] Data based on independent measurements made subsequently to the publication quoted.

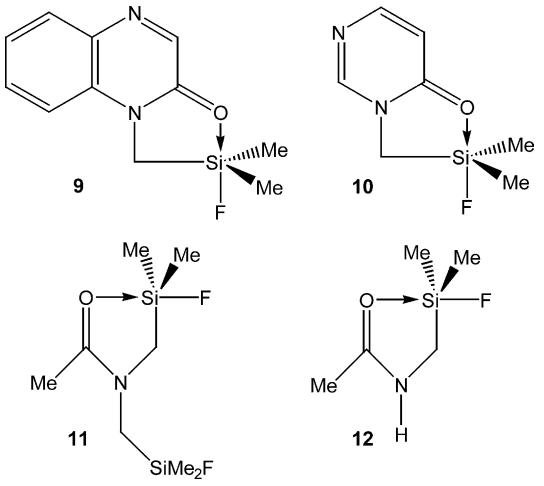

Scheme 5.

Although we are not able to determine the percentage of Nu–Si bond formation for **9**–**12** based on ^{13}C-NMR data, it is still possible to correlate their ^{19}F-NMR chemical shifts and $^{1}J_{Si-F}$ coupling constants with those of **2.1**–**2.6a**, **3.1**–**3.3a**, **4a** and **5a**. While we wish to demonstrate that ^{19}F-NMR chemical shift and coupling constant values can provide quantitative structural information, the primary purpose of this comparison is to show that strong, qualitative interrelations exist between these parameters beyond the complexes originally considered.

Fig. 5 shows that the data for compounds **9**–**12** nests well within the data of the other complexes. The straight line fit excluding **9**–**12** has an R value of 0.96 and including **9**–**12** has a comparable R value of 0.94.

Having established that a linear correlation exists between the ^{19}F-NMR chemical shift and percentage of Nu–Si bond formation it is possible to determine the percentage of Si–F bond formation of each complex based on ^{19}F-NMR chemical shifts. Using the same methodology as for structural correlation with ^{13}C-NMR and ^{29}Si-NMR chemical shifts, each ^{19}F-NMR chemical shift can be placed on a scale between the chemical shifts of limiting structures representing 0 and 100% Si–F bond formation. Trimethylfluorosilane ($\delta^{19}F = -158.0$) was used as the model for 100% Si–F bond formation as it is a good representation of a fully tetrahedral trialkylfluorosilane [14]. The intercept on the y-axis of Fig. 2 suggests a ^{19}F-NMR chemical shift of about −156 for a fluorine fully-bonded to a tetracoordinate, unsubstituted silicon in good agreement with this measured value for Me_3SiF.

For our model of 0% Si–F bond formation we have used our recently prepared compound **13**, the tetrabutylammonium salt of a fluoride ion encapsulated

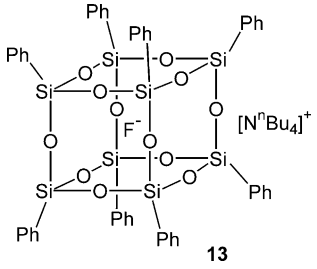

Scheme 6.

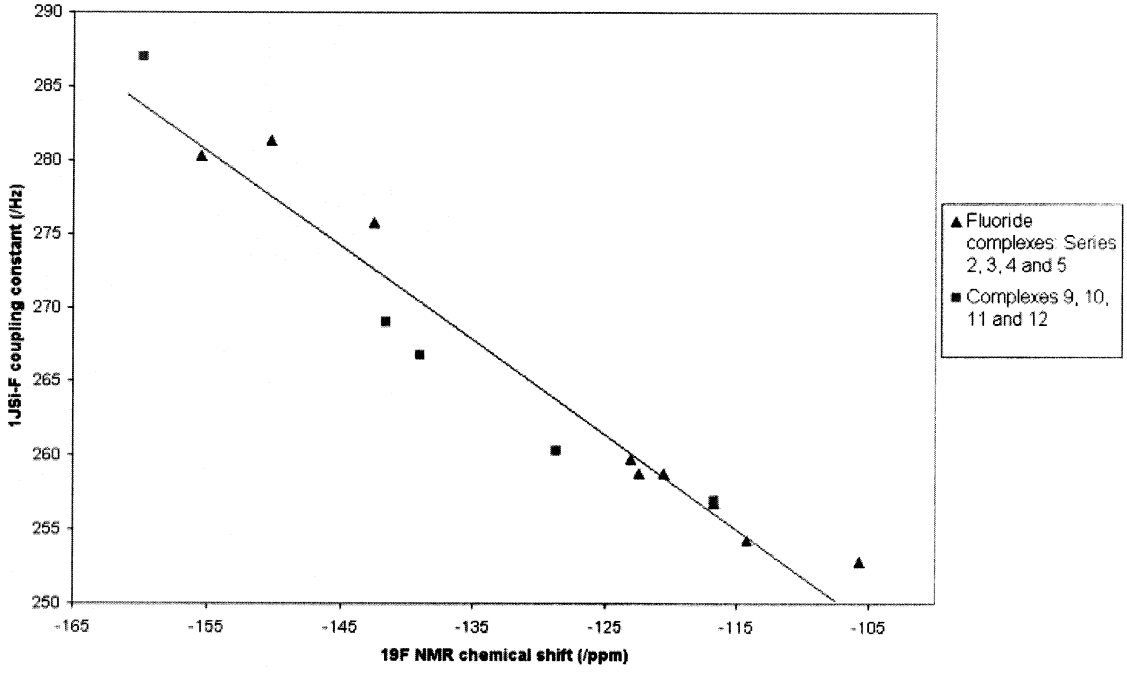

Fig. 5. The plot of $^{1}J_{Si-F}$ NMR coupling constant (Hz) against ^{19}F-NMR chemical shift (ppm) for silyl fluoride complexes of types **2**–**5** and specific complexes **9**–**12**.

within a phenyl-T_8 silsesquioxane cage [15]. While a full discussion of this novel complex will appear elsewhere, it is important to note that the Si–F and O–F inter-atomic distances in the crystal (ranging from 2.65–2.66 to 2.66–2.75 Å, respectively) are too long to be considered formal bonding interactions. In particular the Si–F distances are in excess of the sum of the silicon and fluorine crystal ionic radii (1.98 Å). Solution and solid state ^{19}F-NMR studies on **13** yield a virtually identical chemical shift close to −26 ppm. This is the value we shall therefore use as our benchmark for 0% Si–F bond formation. Interestingly, if the best fit line of the data in Fig. 2 is extrapolated to 100% Nu–Si bond formation the ^{19}F-NMR chemical shift predicted for the fluoride ion at the bonding limit of silicon is in the range −20 to −40 ppm.

The percentage of Si–F bond formation has been calculated based on these limiting values (Table 3) for each of the complexes for which we have previously calculated the percentage of Nu–Si bond formation. A plot of these two values ($R = 0.92$, gradient = −0.99) shows how the increasing Nu–Si bond order is counteracted by a decreasing Si–F bond order and that, within experimental error, the measured sum of percentage of Si–F and Nu–Si bond formation remains constant at a value close to 100%.

Table 5 lists by decreasing O–Si (i.e. Nu–Si) bond length, the relevant inter-atomic distances and angles of a number of reported crystal structures of pentacoordinate silyl fluorides (**2.2a**, **4a**, **11**, **14a** and **15**), chlorides (**4b**, **5b**, **14b**, **16a** and **17-19**), bromides (**4c** and **16b**), iodides (**16c**) and triflates (**4d**). Of these structures data for **2.2a** is reported here for the first time (Table 4). Complex **11** contains both pentacoordinate and tetracoordinate silicon centres and data for both are included in the table. The crystal structures of complexes **5b**, **15** and **18** contain multiple independent molecules (**5.1b**–**5.2b**, **15.1**–**15.4** and **18.1**–**18.2**, respectively) and the data for each is reproduced separately.

As expected, within the series of fluoride complexes, as the Si–O bond length shortens so the Si–F bond tends to extend under the influence of the approaching nucleophile. Table 5 also shows that the distance between the fluorine and the equatorial Si–CH_3 and Si–CH_2 carbons on the silicon gets smaller as the Si–F bond gets longer.

Table 4
A summary of key bond lengths (Å) and bond angles (°) in the crystal of **2.2a**

2.2a			
Bond lengths			
Si–O	1.736(4)	Si–F	1.672(4)
Si–C6	1.893(4)	N–C6	1.468(6)
Si–C7	1.847(6)	C1–O	1.265(5)
Si–C8	1.844(6)	C1–N	1.355(5)
Bond angles			
F–Si–O	171.3(1)	F–Si–C6	91.5(2)
O–Si–C6	79.8(2)	F–Si–C7	97.0(2)
O–Si–C7	87.1(2)	C6–Si–C7	120.5(3)
F–Si–C8	97.9(3)	O–Si–C8	86.8(3)
C6–Si–C8	118.1(2)	C7–Si–C8	118.7(3)

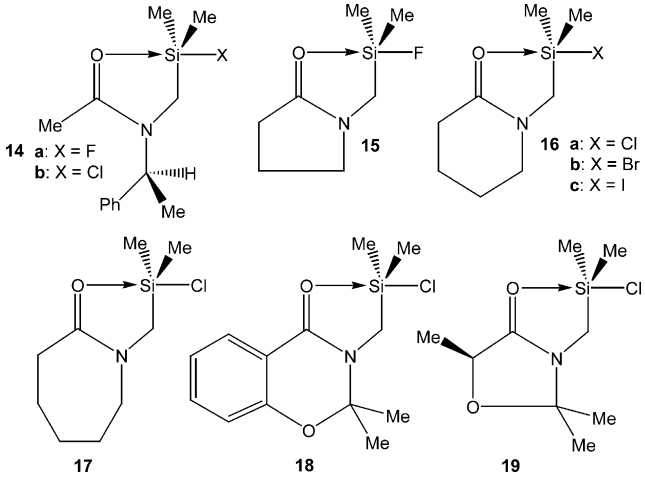

Scheme 7.

Considering all the complexes in Table 5, there is a tendency irrespective of the leaving group X, for the CH_2–X distance and CH_2–Si–X angle to decrease faster than the mean CH_3–X distance and CH_3–Si–X angle during the modelled substitution. A plot of the Si–O bond length against the difference between the mean CH_3–X distance and the actual CH_2–X distance in each complex (Δd) shows an exponential behaviour. A similar behaviour is obtained if the difference between the mean CH_3–Si–F and the actual CH_2–Si–F bond angles in each complex $\Delta\theta$ is plotted against the Si–O bond length. A plot of Δd against $\Delta\theta$, Fig. 6, shows the highly

Table 3
Comparison of the calculated percentage of Si–O and Si–F bond formation for silyl fluoride complexes **2**–**5**

Compound	**2.1a**	**2.2a**	**2.4a**	**2.5a**	**3.1a**	**3.2a**	**3.3a**	**4a**	**5a**
Percentage of Si–O bond formation (A)	30	30	40	20	5	8	7	35	29
δ ^{19}F (ppm)	−116.7	−123.0	−105.7	−122.5	−150.2	−142.5	−155.5	−114.2	−120.5
Percentage of Si–F bond formation (B)	71	76	62	75	97	91	101	69	74
A+B (%)	101	106	102	95	102	99	108	104	103

Table 5
A summary of key crystal structure data from selected pentacoordinate silicon complexes

Compound	X	References	Si–O bond length (Å)	Si–F bond length (Å)	Mean θ_{CH_3-Si-X} (°) (C)	θ_{CH_2-Si-X} (°) (D)	$\Delta\theta$ (°) (C–D)	Mean d_{CH_3-X} distance (Å) (E)	d_{CH_2-X} distance (Å) (F)	Δd (Å) (E–F)
11 (tetra.)	F	[12]	(3.600) [a]	1.603	107.92	107.01	0.91	2.787	2.807	−0.021
15.1	F	[2]	2.461	1.630	101.21	95.14	6.07	2.700	2.606	0.094
15.2	F	[2]	2.451	1.658	100.80	96.72	4.08	2.706	2.649	0.057
19	Cl	[2]	2.425		99.47	94.40	5.07	3.054	2.962	0.092
15.3	F	[2]	2.350	1.665	101.34	95.69	5.65	2.715	2.650	0.065
15.4	F	[2]	2.316	1.656	99.25	93.60	5.65	2.665	2.559	0.106
11 (penta.)	F	[12]	2.187	1.668	98.89	93.30	5.59	2.685	2.590	0.095
14a	F	[16]	2.147	1.668	97.31	93.38	3.93	2.648	2.594	0.054
2.2a	F		2.115	1.671	97.45	91.54	5.91	2.645	2.559	0.086
4a	F	[4]	2.065	1.675	97.08	90.83	6.25	2.652	2.550	0.102
18.1	Cl	[2]	1.990		94.05	87.58	6.47	3.058	2.918	0.140
18.2	Cl	[2]	1.989		94.08	88.62	5.46	3.066	2.956	0.110
14b	Cl	[16]	1.974		93.09	88.26	4.83	3.040	2.939	0.101
16a	Cl	[2]	1.954		93.46	87.96	5.50	3.051	2.930	0.121
17	Cl	[2]	1.950		93.40	88.31	5.09	3.055	2.947	0.108
4b	Cl	[4]	1.939		93.86	87.32	6.54	3.072	2.928	0.144
5.1b	Cl	[7]	1.937		93.70	87.80	5.90	3.068	2.943	0.125
5.2b	Cl	[7]	1.923		94.37	86.96	7.41	3.076	2.908	0.168
4c	Br	[4]	1.852		89.97	82.90	7.07	3.231	3.058	0.173
16b	Br	[2]	1.800		87.88	74.69	13.19	3.569	3.185	0.384
16c	I	[2]	1.749		82.86	71.96	10.90	3.951	3.624	0.327
4d	O-Tf	[4]	1.745		84.49	71.01	13.48	3.168	2.790	0.378

[a] The shortest non-bonding $Si_{tetra.}$ contact distance in the crystal (intermolecular Si···HC).

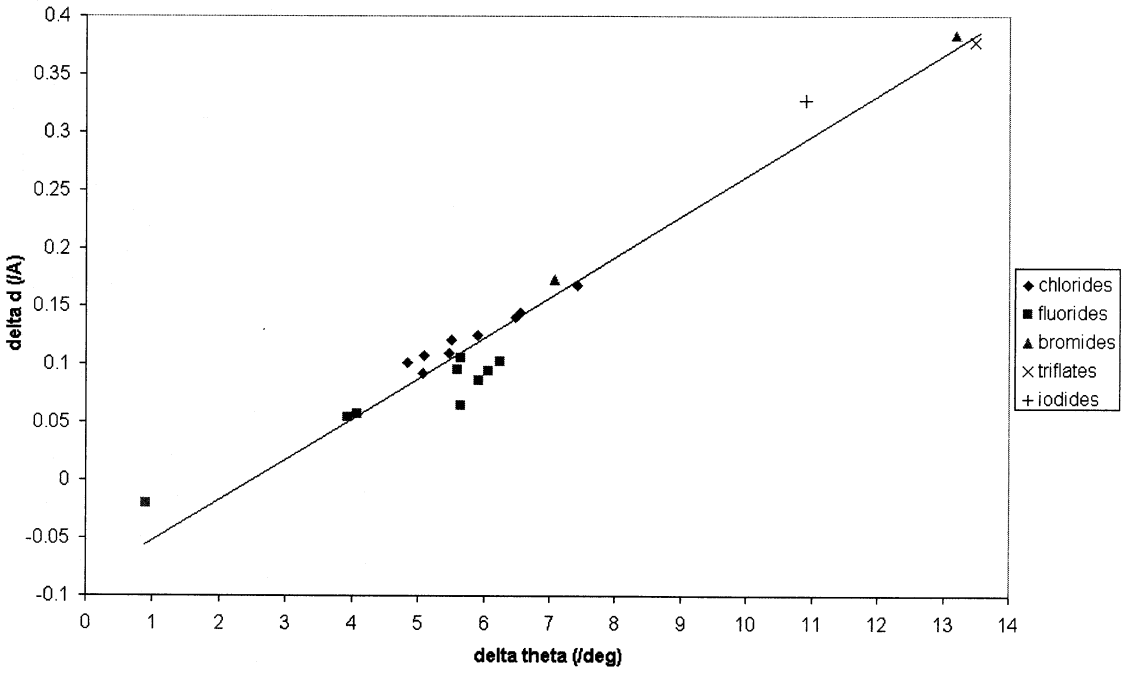

Fig. 6. The plot of Δd (Å) against $\Delta\theta$ (°) for selected pentacoordinate silicon complexes.

correlated ($R = 0.96$) nature of the net distortion of the leaving group towards the Si–CH_2 group. This distortion trend in the solid state may explain why the $^2J_{C-F}$ NMR coupling constants for the Si–CH_2 carbons of fluorosilane complexes increase more rapidly than those of the Si–CH_3 carbons due to an increasing through-space coupling component.

While the overall trends in the crystal structure data allow us to elucidate much about the mechanism we are studying, some deviations from the line of best fit are clearly observed for individual structures and substructures. Deformation of the molecules from their isolated, equilibrium structures due to crystalline packing effects probably plays an important part in accounting for many of these deviations.

3. Conclusion

The well-proven technique of solution phase mapping of nucleophilic substitution at silicon has been extended to include measuring its trajectory from ^{19}F-NMR chemical shift data in a series of five-coordinate silyl–monofluoride complexes. We have also shown that the $^1J_{Si-F}$ and $^2J_{C-F}$ NMR coupling constants are closely related to the substitution process and therefore can also be used to elucidate information about their structures.

During the modelled substitution the $^1J_{Si-F}$ coupling constant was found to decrease and the $^2J_{C-F}$ coupling constants were found to increase, with the coupling to the Si–CH_2 carbon increasing faster than to the Si–CH_3 carbons. We have suggested that differences in the hybridisation state of the silicon between complexes affects the Fermi contact mechanism of through-bond coupling and may therefore be important in controlling the magnitude of the $^1J_{Si-F}$ coupling constant. As the leaving group ability of fluorine is relatively low, compared with the other leaving groups we have used in our studies, all of the silyl fluoride structures are found at the lower end of the substitution range between 0 and 50% Nu–Si bond formation. However, across this range the pattern of data is consistent with an increasingly trigonal-bipyramidal silicon with strengthening Nu–Si bond.

By pooling the X-ray crystal structure data for many of our pentacoordinate silicon complexes together with related structures in the literature we have been able to provide a possible explanation of why the $^2J_{C-F}$ NMR coupling constants increase during the first half of our modelled substitution for silyl fluorides based on a faster decrease in through-space contact distances accompanied by faster decreasing C–Si–F bond angles for the Si–CH_2 carbon than for the Si–CH_3 carbons. This progressive distortion of the leaving group's path seems to be independent of the leaving group and inherently due to the enforced non-ideal approach trajectory of the nucleophile caused by the modelled substitution taking place intramolecularly in each complex we considered.

4. Experimental

All ^{19}F-NMR measurements were made on either JEOL FX90Q or EX400 FT machines fitted with

multinuclear probes. Spectra were recorded at 20 °C using $CDCl_3$ dried over 4A molecular sieves as solvent and an external reference of $CFCl_3$. The data presented here is limited mainly to that reported for the first time in this publication. References are made as appropriate to the source of previous publication and characterisation of each compound.

*4.1. 1-(Fluorodimethylsilylmethyl)-2-pyridone (**2.1a**)[4]*

δ_F(90 MHz) −116.7.

*4.2. 1-(Fluorodimethylsilylmethyl)-5-chloro-2-pyridone (**2.2a**)[4]*

δ_F(90 MHz) −123.0.

*4.3. 1-(Fluorodimethylsilylmethyl)-6-methyl-2-pyridone (**2.4a**)[4]*

δ_F(90 MHz) −105.7.

*4.4. 1-(Fluorodimethylsilylmethyl)-3-methoxy-2-pyridone (**2.5a**)[4]*

δ_F(90 MHz) −122.5.

*4.5. N,N-bis(fluorodimethylsilylmethyl)acetamide (**11**)[12]*

δ_F(90 MHz) −159.8 (Si_{tetra}), −116.7 (Si_{penta}).

*4.6. N-(fluorodimethylsilylmethyl)acetamide (**12**)[13]*

δ_F(90 MHz) −139.0.

Acknowledgements

We would like to thank the EPSRC for funding D.J.P. and the Russian Foundation for Basic Research (Project 01-03-32216) for funding V.V.N. We would also like to thank Dr Keith Pannell for the crystal structure data of compound **2.2a**.

References

[1] (a) D. Britton, J.D. Dunitz, J. Am. Chem. Soc. 103 (1981) 2971; (b) H.B. Bürgi, J.D. Dunitz, Acc. Chem. Res. 16 (1983) 153.
[2] (a) A.A. Macharashvili, V.E. Shlover, N.Y. Chernikova, M.Y. Antipin, Y.T. Struchkov, Y.I. Baukov, G.I. Oleneva, E.P. Kramarova, A.G. Shipov, J. Organomet. Chem. 359 (1989) 13; (b) A.A. Macharashvili, V.E. Shlover, Y.T. Struchkov, G.I. Oleneva, E.P. Kramarova, A.G. Shipov, Y.I. Baukov, J. Chem. Soc. Chem. Commun. (1988) 683.
[3] V.F. Sidorkin, V.V. Vladimirov, M.G. Voronkov, V.A. Pestunovich, J. Mol. Struct. (Theochem.) 228 (1991) 1.
[4] A.R. Bassindale, M. Borbaruah, S.J. Glynn, D.J. Parker, P.G. Taylor, J. Chem. Soc. Perkin Trans. 2 (1999) 2099.
[5] (a) A.R. Bassindale, M. Borbaruah, J. Chem. Soc. Chem. Commun. (1991) 1499.; (b) A.R. Bassindale, M. Borbaruah, J. Chem. Soc. Chem. Commun. (1991) 1501.
[6] A.R. Bassindale, D.J. Parker, P.G. Taylor, J. Chem. Soc. Perkin Trans. 2 (2000) 1059.
[7] A.R. Bassindale, S.J. Glynn, P.G. Taylor, N. Auner, B. Herrschaft, J. Organomet. Chem. 619 (2001) 132.
[8] A.R. Bassindale, D.J. Parker, P.G. Taylor, N. Auner, B. Herrschaft, J. Organomet. Chem. (2003), in press.
[9] R.J.P. Corriu, C. Guerin, J. Organomet. Chem. 198 (1980) 231.
[10] K. Tamao, T. Hayashi, Y. Ito, M. Shiro, Organometallics 11 (1992) 2099.
[11] S.E. Johnson, J.S. Payne, R.O. Day, J.M. Holmes, R.R. Holmes, Inorg. Chem. 28 (1989) 3190.
[12] A.G. Shipov, E.P. Kramarova, E.A. Mamaeva, O.A. Zamyshlyaeva, V.V. Negrebetsky, Y.E. Ovchinnikov, S.A. Pogozhikh, A.R. Bassindale, P.G. Taylor, Y.I. Baukov, J. Organomet. Chem. 620 (2001) 139.
[13] Y.I. Baukov, O.A. Zamyshlyaeva, S.A. Pogozhikh, E.P. Kramarova, A.G. Shipov, V.V. Negrebetsky, Y.E. Ovchinnikov, Russ. Chem. Bull. 48 (1999) 1796.
[14] G. Englehardt, K. Licht, Z. Chem. 10 (1970) 266.
[15] A.R. Bassindale, M. Pourny, P.G. Taylor, unpublished results.
[16] Y.I. Baukov, Y.E. Ovchinnikov, A.G. Shipov, E.P. Kramarova, V.V. Negrebetsky, Y.T. Struchkov, J. Organomet. Chem. 536–537 (1997) 399.